

基于 Rb^{87} 调制转移光谱稳频技术研究洪毅^{1,2}, 侯霞^{1*}, 陈迪俊^{1,3}, 周翠芸¹, 黄敏捷¹, 宋铁强¹, 王桂冰¹, 赵剑¹, 陈卫标¹¹中国科学院上海光学精密机械研究所航天激光工程部, 上海 201800;²中国科学院大学, 北京 100049;³国科大杭州高等研究院, 浙江 杭州 310024

摘要 相对于传统的 780 nm 饱和吸收光谱稳频技术, 调制转移光谱法具有更高的灵敏度和分辨率。采用调制转移光谱技术将 1560 nm 分布式反馈激光器经全光纤放大和 PPLN 晶体高效倍频至 780 nm 后锁定在 Rb^{87} 原子 D_2 线超精细谱线 $5^2S_{1/2}(F_g=1) \rightarrow 5^2P_{3/2}(F_e=0,1)$ 交叉共振峰上, 20 h 激光器的频率漂移峰峰值为 105 kHz, 1 s 的阿伦方差为 3.7×10^{-11} , 10000 s 的阿伦方差为 4.6×10^{-12} 。研究了铷泡吸收长度对频率稳定性的影响。针对 Rb^{87} $5^2S_{1/2}(F_g=1) \rightarrow 5^2P_{3/2}(F_e=0,1,2)$ 吸收峰较弱问题, 研究了不同偏振类型的泵浦光和探测光对误差信号的影响。

关键词 激光光学; 激光稳频; 调制转移光谱技术; 反馈光; 偏振; 超冷原子

中图分类号 TN249

文献标志码 A

doi: 10.3788/CJL202148.2101003

1 引言

自由运转状态下激光器容易受外界因素例如温度、气压、振动、噪声等影响, 从而改变激光器谐振腔几何长度和腔内介质折射率, 使得激光器频率抖动过大, 无法满足应用需求。因此, 想要获得稳定的激光波长, 需对激光器采用稳频技术^[1-4]。稳频的基本原理是将激光器频率锁定在某个稳定的参考频率上, 如原子以及分子的跃迁谱线上^[5]。常用的稳频方法有原子双向色性稳频技术(DAVLL)法^[6]、偏振光谱法^[7]、频率调制法^[8]、Pound-Drever-Hall (PDH)法^[9]、饱和吸收光谱法^[10]、调制转移光谱(MTS)法^[11]等。相对于应用较广的饱和吸收光谱法, MTS 可以产生类似的四波混频效应, 泵浦光的调制信息将被转移到探测光束中, 进而被光电探测器接收, 通过后续解调得到稳频所需的误差信号。由于调制转移严格发生在多普勒速度为零的分子或原子间, 因此解调的误差信号没有多普勒背景, 避免了对激光器直接加调制带来的附加噪声, 具有高灵敏高分辨率, 以及误差信号斜率高等优点, 且对温度和功率的抖动不敏感, 非常适合用来激光稳频^[12]。

目前国内外文献关于 Rb^{87} 调制转移光谱稳频技术的研究大多将 D_2 线的超精细谱线 $5^2S_{1/2}(F_g=2) \rightarrow 5^2P_{3/2}(F_e=3)$ 作为锁频谱线。2009 年, Qi 等^[13]采用 MTS 技术对 Rb^{87} 的 $5^2S_{1/2}(F_g=2) \rightarrow 5^2P_{3/2}(F_e=3)$ 跃迁实现稳频, 测得的频率稳定性结果为 $3.9 \times 10^{-13} @ 1 \text{ s}$ 和 $9.8 \times 10^{-14} @ 90 \text{ s}$ 。2014 年, 山西大学韩亚帅等^[14]研究了频率调制法和 MTS 分别将 Rb^{87} 锁定在 $5^2S_{1/2}(F_g=2) \rightarrow 5^2P_{3/2}(F_e=3)$ 跃迁上频率稳定性的差别。2020 年, 华中光电技术研究所的栾广建等^[15]采用 MTS 将 Rb^{87} 锁定在 $5^2S_{1/2}(F_g=2) \rightarrow 5^2P_{3/2}(F_e=3)$ 跃迁上, 实现 20 h 不失锁。然而文献中关于 Rb^{87} 原子 D_2 线的超精细谱线 $5^2S_{1/2}(F_g=1) \rightarrow 5^2P_{3/2}(F_e=0,1,2)$ 作为频率跃迁谱线的研究报道较少。究其原因, 主要是后者的饱和吸收峰和误差信号幅度相比前者小得太多。2011 年, Noh 等^[16]研究了探测光和泵浦光均为同向线偏振光时 Rb^{87} 在 $5^2S_{1/2}(F_g=1) \rightarrow 5^2P_{3/2}(F_e=0,1,2)$ MTS 的光谱误差信号线型。由于 Rb^{87} D_2 线的超精细谱线 $5^2S_{1/2}(F_g=1) \rightarrow 5^2P_{3/2}(F_e=0,1)$ 真空中频率为 384234490.2 MHz, 适用

收稿日期: 2021-02-03; 修回日期: 2021-03-22; 录用日期: 2021-04-15

通信作者: *hy1989_0629@126.com

于冷原子钟系统冷却 Rb^{87} 原子所需的重泵浦光,具有非常重大的研究意义。

本文采用 1560 nm 窄线宽分布式反馈(DFB)半导体激光器作为种子源,通过主振荡功率放大^[17](MOPA)技术得到功率放大,经过 PPLN 倍频晶体之后得到 780 nm 激光,利用 MTS 技术稳定在 Rb^{87} D_2 线的超精细谱线 $5^2S_{1/2}(F_g=1) \rightarrow 5^2P_{3/2}(F_e=0,1)$ 交叉共振峰上。针对 Rb^{87} $5^2S_{1/2}(F_g=1) \rightarrow 5^2P_{3/2}(F_e=0,1,2)$ 吸收峰较弱的问题,理论分析了不同偏振类型的泵浦光和探测光对 MTS 误差信号线型不同的原因。为使误差信号达到更好的信噪比,研究了铷泡吸收长度对频率稳定性的影响。

2 实验原理

激光器经过电光调制器后可以表示为 $\omega = \omega_0 + \beta \cos(\omega_m t)$,其中 ω 为激光器瞬时频率, ω_0 为激光器中心频率, ω_m 为调制频率, β 为频率调制幅度。

经过调制后光场可以表示为

$$E(t) = E_0 \exp\{i[\omega_0 + \beta \cos(\omega_m t)]t\} \approx E_0 \exp\{i[\omega_0 t + M \sin(\omega_m t)]\}, \quad (1)$$

$$M = \pi l n_e^3 r_{33} V / \lambda h, \quad (2)$$

式中: E_0 为光场振幅; l 为调制晶体长度; n_e 为调制晶体对 e 光折射率; r_{33} 为调制晶体介电常数; V 为调制频率幅度; h 为调制晶体高度; M 为调制深度。

则(1)式可以用贝塞尔函数表示为

$$E(t) = E_0 \exp(i\omega_0 t) \sum_{n=-\infty}^{n=\infty} J_n(M) \exp(in\omega_m t). \quad (3)$$

经过调制的泵浦光和未经调制的探测光在原子气室共线方向传播,当满足亚多普勒共振条件时,发生类四波混频效应,在弱探测光上产生调制,探测光经过原子气室后进入光电探测器。探测器探测到的信号和本地振荡混频后得到的信号如下,

$$S(\omega_m) = \frac{C}{\sqrt{\Gamma^2 + \omega_m^2}} \sum_{n=-\infty}^{\infty} J_n(M) J_{n-1}(M) \times [(L_{(n+1)/2} + L_{(n-2)/2}) \cos(\omega_m t + \varphi) + (D_{(n+1)/2} - D_{(n-2)/2}) \sin(\omega_m t + \varphi)], \quad (4)$$

式中: $J_n(M)$ 为 n 阶贝塞尔函数; φ 为作用在泵浦光的调制相位; C 为信号幅度的参数,主要取决于探测器的参数及激光强度; L_n 为洛伦兹线性(吸收线性); D_n 为色散线性。

$$L_n = \frac{\Gamma^2}{\Gamma^2 + (\Delta - n\omega_m)^2}, \quad (5)$$

$$D_n = \frac{\Gamma(\Delta - n\omega_m)}{\Gamma^2 + (\Delta - n\omega_m)^2}, \quad (6)$$

式中: Δ 为激光频率相对共振频率的失谐; Γ 为原子自然线宽;对于 Rb^{87} 原子,其 D_2 线的自然线宽为 6 MHz。当调制深度 $M < 1$,上式可以简化为

$$S(\omega_m) = \frac{C}{\sqrt{\Gamma^2 + \omega_m^2}} J_0(M) J_1(M) \times [(L_{-1} - L_{-1/2} + L_{1/2} - L_1) \cos(\omega_m t + \varphi) + (D_1 - D_{1/2} - D_{-1/2} + D_{-1}) \sin(\omega_m t + \varphi)]. \quad (7)$$

可以看出,当调制频率 $\omega_m \leq \Gamma$ 时,吸收项和色散项有着相同的类色散线型,都可以作为误差信号来稳定激光器。

3 实验装置

利用 MTS 的稳频实验如图 1 所示,ISO 为隔离器,combiner 为合束器,Er-fiber 为掺 Er^{3+} 增益光纤,PPLN 为倍频晶体,PBS 为偏振分光棱镜, $\lambda/2$ 为半波片,铷泡直径 10 mm,长度为 50 mm,PIN 为光电探测器,AMP 为功率放大器,MIX 是混频器,SG 为信号发生器,LPF 为低通滤波器,PID 是比例-积分-微分控制器。

采用 MOPA 放大技术对 1560 nm 种子激光器进行功率放大。种子源为 Emcore 公司生产的 DFB 激光器,最大输出功率为 100 mW,线宽为 1 MHz,通过改变激光器的工作温度和注入电流,可以实现 1557~1560 nm 波长的调谐,实验中激光器工作温度为 39.8 °C,注入电流为 191 mA,工作波长为 1560.48 nm,出光功率为 22 mW。经过光学隔离器后和泵浦光一起进入合束器。泵浦光为北京凯普林光电科技股份有限公司生产的 940 nm 激光光源,最大输出功率为 10 W,实验中注入电流为 1.5 A,输出功率为 1.2 W。经过掺 Er^{3+} 增益光纤后,最终输出 500 mW 的 1560 nm 激光。输出光进入 PPLN 倍频晶体,通过改变倍频晶体温度可以实现 1560 nm 向 780 nm 高效转化,最终 PPLN 倍频晶体控温在 61.4 °C,780 nm 激光输出功率为 200 mW,随后通过分束器,10%功率用于 Rb^{87} 调制转移光谱稳频实验。

进入稳频实验的 780 nm 激光通过一个 1:3 的分束器将光束分成两路,其中 25% 作为探测光,75% 作为泵浦光。探测光经过一个二分之一波片和偏振分光棱镜进入铷泡,泵浦光先经过一个电光相位调制器(调制频率为 4 MHz),再通过一个二分之一波片和两个偏振分光棱镜反向进入铷泡,调节二

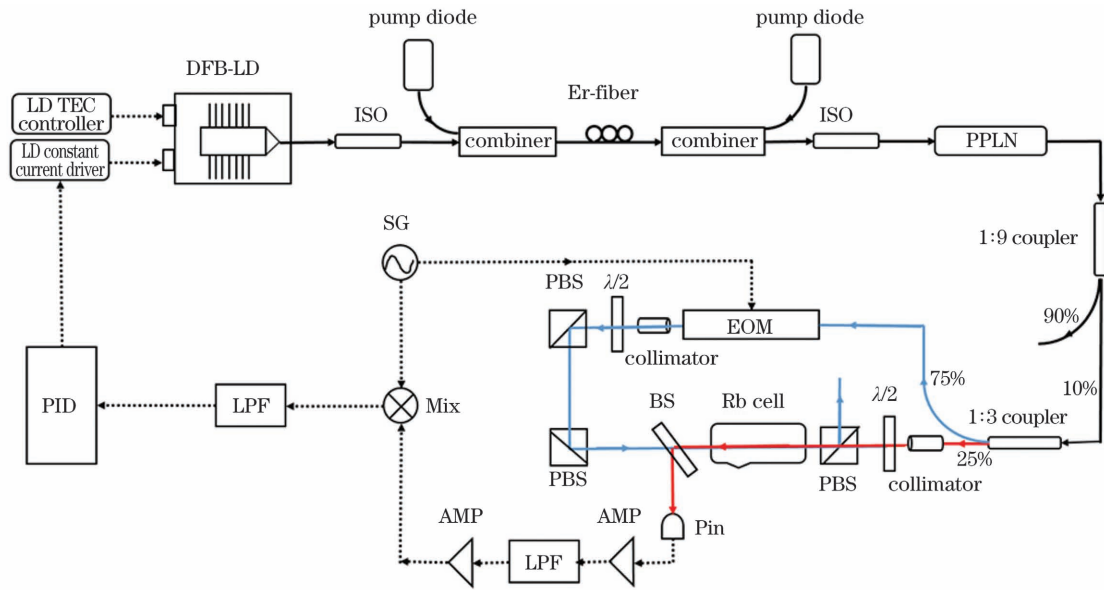


图 1 MTS 的实验装置示意图

Fig. 1 Diagram of the experimental setup for MTS

分之一波片可以改变探测光和泵浦光进入铷泡的功率大小,实验中探测光功率为 $50 \mu\text{W}$, 泵浦光功率为 $150 \mu\text{W}$ 。两束激光在铷泡里重叠,发生四波混频效应,探测光通过一个分光棱镜进入光电探测器中。通过调节激光器电流和加在电流调制端口电压的幅度,可得到 Rb^{87} 的 $5^2\text{S}_{1/2} \rightarrow 5^2\text{P}_{3/2}$ 跃迁的 $F_g = 1 \rightarrow F_e = 0, 1, 2$ 以及 $F_g = 2 \rightarrow F_e = 1, 2, 3$ 饱和吸收峰。Pin 管的输出信号经过低噪声功率放大器 and 截止频率为 4 MHz 的低通滤波器后输入到混频器中与移相后的本振信号进行解调。混频器输出的解调信号经过截止频率为 100 kHz 的低通滤波器后,即得到所需要的误差信号。误差信号最终被输入到 PID 控制电路中用于稳频。

4 实验结果与讨论

4.1 不同偏振方向的探测光和泵浦光对 $\text{Rb}^{87} 5^2\text{S}_{1/2} \rightarrow 5^2\text{P}_{3/2} F_g = 1 \rightarrow F_e = 0, 1, 2$ 误差信号的影响

如图 2 所示,实验测得 $\text{Rb}^{87} \text{D}_2$ 线的超精细谱线 $5^2\text{S}_{1/2} \rightarrow 5^2\text{P}_{3/2} F_g = 2 \rightarrow F_e = 1, 2, 3$ 以及 $F_g = 1 \rightarrow F_e = 0, 1, 2$ 的饱和吸收峰和 MTS 误差信号,可以明显看出后者的信号幅值比前者小得多。为了更好地将系统中的重泵浦光频率锁定在 $\text{Rb}^{87} \text{D}_2$ 线的超精细谱线 $5^2\text{S}_{1/2} (F_g = 1) \rightarrow 5^2\text{P}_{3/2} (F_e = 0, 1)$ 交叉共振峰上,需对其误差信号幅值进行优化。

通过改变稳频光路结构,研究了探测光和泵浦光分别为同向线偏振光、垂直方向线偏振光、圆偏振光三种状态下,调制转移光谱在 $\text{Rb}^{87} F_g = 1 \rightarrow F_e =$

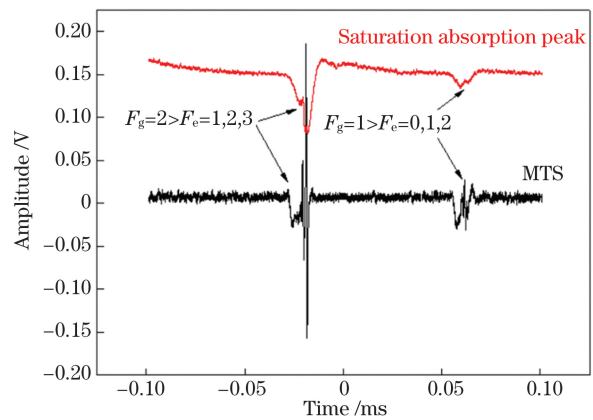


图 2 $\text{Rb}^{87} 5^2\text{S}_{1/2} \rightarrow 5^2\text{P}_{3/2}$ 跃迁的 $F_g = 2 \rightarrow F_e = 1, 2, 3$ 以及 $F_g = 1 \rightarrow F_e = 0, 1, 2$ 的饱和吸收峰和 MTS 误差信号

Fig. 2 $\text{Rb}^{87} 5^2\text{S}_{1/2} \rightarrow 5^2\text{P}_{3/2}$ transition $F_g = 2 \rightarrow F_e = 1, 2, 3$, and $F_g = 1 \rightarrow F_e = 0, 1, 2$ saturated absorption peak and MTS error signal

$0, 1, 2$ 误差信号线型。实验结果如图 3 所示。当探测光和泵浦光为同向线偏振光时,MTS 误差信号没有发现 $F_g = 1 \rightarrow F_e = 1$ 跃迁和非常微弱的 $F_g = 1 \rightarrow F_e = 0$ 跃迁(虽然这也是个循环跃迁,类似于 $F_g = 2 \rightarrow F_e = 3$)。但在 $F_g = 1 \rightarrow F_e = 0, 1$ 的交叉共振峰处却有个大信号。当探测光和泵浦光为垂直方向线偏振光时,MTS 误差信号没有 $F_g = 1 \rightarrow F_e = 1$ 跃迁,但在 $F_g = 1 \rightarrow F_e = 0$ 和 $F_g = 1 \rightarrow F_e = 0, 1$ 的交叉共振峰处都有较强信号。当探测光和泵浦光为圆偏振光时,MTS 误差信号类似于探测光和泵浦光为垂直方向线偏振光的情况,但信号幅值几乎是后者的一半。

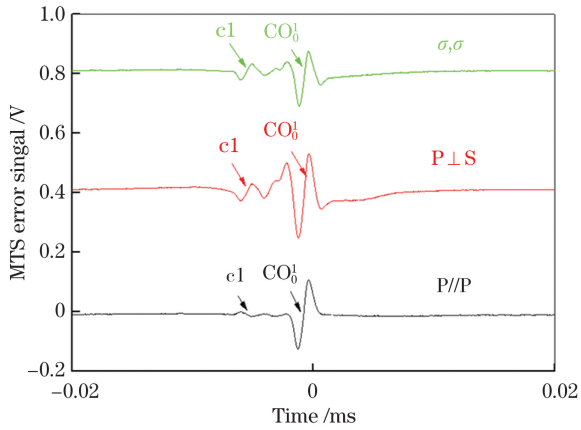


图 3 三种偏振状态的探测光和泵浦光在 $\text{Rb}^{87} F_g = 1 \rightarrow F_e = 0, 1, 2$ 的 MTS 误差信号

Fig. 3 MTS error signals of probe beam and pump beam in $\text{Rb}^{87} F_g = 1 \rightarrow F_e = 0, 1, 2$ for three polarization states

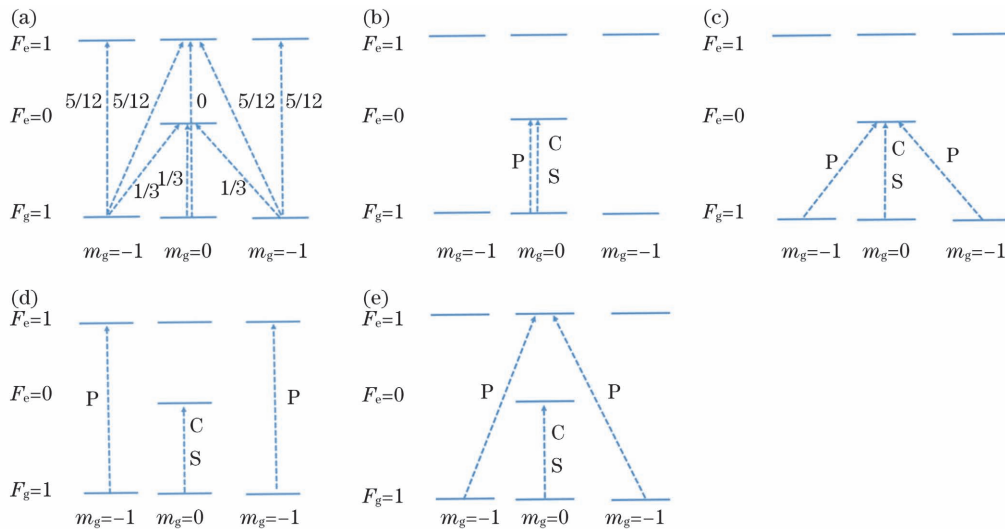


图 4 $\text{Rb}^{87} 5^2 S_{1/2} \rightarrow 5^2 P_{3/2}$ 能级跃迁图。(a) $F_g = 1 \rightarrow F_e = 0, 1, 2$ 跃迁的归一化强度；(b) (c) 探测光和泵浦光为同向和垂直方向线偏振光 $F_g = 1 \rightarrow F_e = 0$ 跃迁示意图；(d) (e) 探测光和泵浦光为同向和垂直方向线偏振光 $F_g = 1 \rightarrow F_e = 0, 1$ 跃迁示意图

Fig. 4 Energy level diagrams for the transitions $5^2 S_{1/2} \rightarrow 5^2 P_{3/2}$ of Rb^{87} . (a) Normalized intensity of $F_g = 1 \rightarrow F_e = 0, 1, 2$; (b) (c) energy level diagrams for the transitions $F_g = 1 \rightarrow F_e = 0$ where probe light and pump light are linearly polarized light in the same direction and vertical direction, respectively; (d) (e) energy level diagrams for the transitions $F_g = 1 \rightarrow F_e = 0, 1$ probe light and pump light are linearly polarized light in the same direction and vertical direction, respectively

对于 $F_g = 1 \rightarrow F_e = 0, 1$ 的交叉共振峰, 三种偏振态都有很大的 MTS 误差信号, 同向线偏振光和垂直方向线偏振信号幅值大致相同, 圆偏振光的信号幅值仍是垂直方向线偏振光的一半。当探测光和泵浦光为同向线偏振光时, 泵浦光(C)和边带(S)由基态 $|F_g = 1, m_g = 0\rangle$ 光泵到了激发态 $|F_e = 0, m_e = 0\rangle$, 而探测光(P)由基态 $|F_g = 1, m_g = \pm 1\rangle$ 光

对于 $F_g = 1 \rightarrow F_e = 0$ 跃迁, 当探测光和泵浦光为同向线偏振光时, 基态 $|F_g = 1, m_g = 0\rangle$ 先被光泵到了激发态 $|F_e = 0, m_e = 0\rangle$, 再自发辐射到了基态 $|F_g = 1, m_g = \pm 1\rangle$, 虽然这是个循环跃迁, 但由于基态 $|F_g = 1, m_g = 0\rangle$ 布居数的减少, 导致其误差信号幅值非常微弱。当探测光和泵浦光为垂直方向线偏振光时, MTS 误差信号的产生可以这样理解, 泵浦光(C)和边带(S)由基态 $|F_g = 1, m_g = 0\rangle$ 光泵到了激发态 $|F_e = 0, m_e = 0\rangle$, 而探测光(P)由基态 $|F_g = 1, m_g = \pm 1\rangle$ 光泵到了激发态 $|F_e = 0, m_e = 0\rangle$, 基态 $|F_g = 1, m_g = 0, \pm 1\rangle$ 到激发态 $|F_e = 0, m_e = 0\rangle$ 的归一化强度均为 $1/3$, MTS 误差信号可以由基态 $|F_g = 1, m_g = \pm 1\rangle$ 产生。垂直方向线偏振光可以看作是左旋圆偏振光和右旋圆偏振光的叠加, 所以探测光和泵浦光是圆偏振态的 MTS 误差信号幅值是垂直方向线偏振光的一半。

泵到了激发态 $|F_e = 0, m_e = \pm 1\rangle$; 当探测光和泵浦光为垂直方向线偏振光时, 泵浦光(C)和边带(S)由基态 $|F_g = 1, m_g = 0\rangle$ 光泵到了激发态 $|F_e = 0, m_e = 0\rangle$, 而探测光(P)由基态 $|F_g = 1, m_g = \pm 1\rangle$ 光泵到了激发态 $|F_e = 1, m_e = 0\rangle$ 。基态 $|F_g = 1, m_g = \pm 1\rangle$ 跃迁到激发态 $|F_e = 1, m_g = 0, \pm 1\rangle$ 的归一化强度均为 $5/12$, 所以两者 MTS 误差信号幅度

相当。

对于 $F_g=1 \rightarrow F_e=1$ 跃迁, 三种偏振态都没有观察到 MTS 误差信号, 这是因为基态 $|F_g=1, m_g=0\rangle$ 跃迁到激发态 $|F_e=1, m_g=0\rangle$ 的归一化强度均为 0, 所以没有信号产生。

实验最终采用同向线偏振光的探测光和泵浦光的光路结构, 原因是相对于垂直方向线偏振光结构, 前者的 MTS 误差信号在 $5^2S_{1/2}(F_g=1) \rightarrow 5^2P_{3/2}(F_e=0, 1)$ 交叉共振峰上背景干净, 只有单一的信号, 不会出现锁错峰的情况。相对于圆偏振光结构, 其 MTS 误差信号幅值更大, 具有更好的信噪比。

4.2 铷泡吸收长度对稳频性能的影响

铷泡吸收长度会影响 MTS 误差信号的幅值, 从而影响误差信号的信噪比和频率稳定性。采用气压均为 4×10^{-5} Pa, 通光口径均为 10 mm, 长度分别为 25 mm 和 50 mm 的两种规格铷泡进行实验。在相同实验条件下得到的误差信号如图 5 所示。

可以明显地观察到长度为 50 mm 的铷泡 MTS 误差信号幅值大于 25 mm 的铷泡, 前者为 980 mV, 后者为 710 mV。通过 PID 控制电路将激光频率锁定在 $Rb^{87} D_2$ 线的超精细谱线 $5^2S_{1/2}(F_g=1) \rightarrow 5^2P_{3/2}(F_e=0, 1)$ 交叉共振峰上, 激光器的频率稳定性由光梳 (Menlo systems 公司的 FC1500-250-WG 掺铒光学频率梳系统, 采用锁模技术生成超快激光光源, 锁定在内置铷钟频率上, 实现良好的稳定性, 稳定性阿伦方差 1 s 积分时间 $< 2 \times 10^{-11}$, 100 s 积分时间 $< 2 \times 10^{-12}$) 测得, 实验结果如图 6 所示。图 6 显示 50 mm 铷泡 1 h 频率变化量为 80 kHz, 小

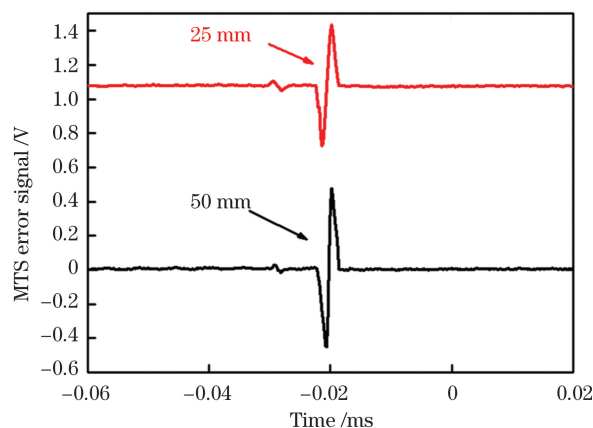


图 5 长度为 25 mm 和 50 mm 铷泡在 $Rb^{87} F_g=1 \rightarrow F_e=0, 1, 2$ 的 MTS 误差信号

Fig. 5 MTS error signals of 25 mm and 50 mm rubidium cell in $Rb^{87} F_g=1 \rightarrow F_e=0, 1, 2$

于 25 mm 铷泡 1 h 频率变化量 (152 kHz), 其 1 s 的频率稳定度为 3.7×10^{-11} 同样小于 25 mm 铷泡 (5.4×10^{-11}), 但两者的 1000 s 频率稳定度相差不多, 分别为 1.2×10^{-11} 和 1.4×10^{-11} 。表明适当增加单个铷泡吸收长度对改善误差信号信噪比是有利的, 能提高激光器短期内频率稳定性。

最终采用 50 mm 铷泡规格, 将激光器频率锁定在 $Rb^{87} D_2$ 线的超精细谱线 $5^2S_{1/2}(F_g=1) \rightarrow 5^2P_{3/2}(F_e=0, 1)$ 交叉共振峰上, 结果如图 7 所示, 20 h 频率漂移峰峰值为 105 kHz, 积分时间为 1 s 的阿伦方差为 3.7×10^{-11} , 10000 s 的阿伦方差为 4.6×10^{-12} , 测得的绝对频率为 384234489.5 MHz (理论推算应为 384234490.2 MHz, 相差 0.7 MHz)。满足系统对频率稳定的性能指标。

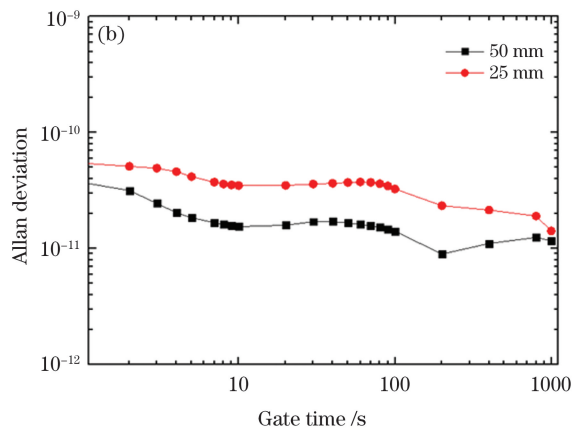
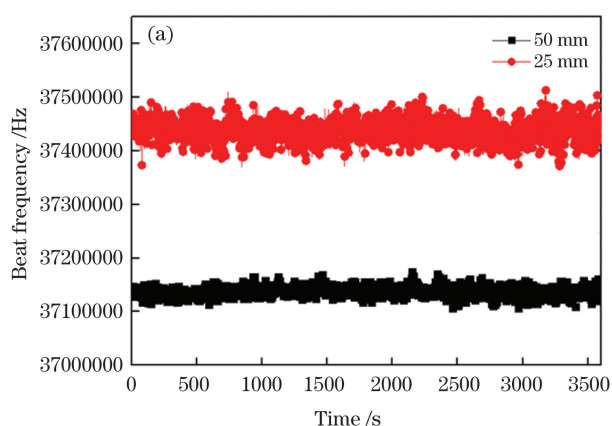


图 6 25 mm 和 50 mm 铷泡实验结果。(a) 1 h 的稳频频率漂移; (b) 1000 s 时的阿伦方差

Fig. 6 Experimental results of 25 mm and 50 mm rubidium cells. (a) Frequency fluctuation in 1 h; (b) Allan deviation within 1000 s

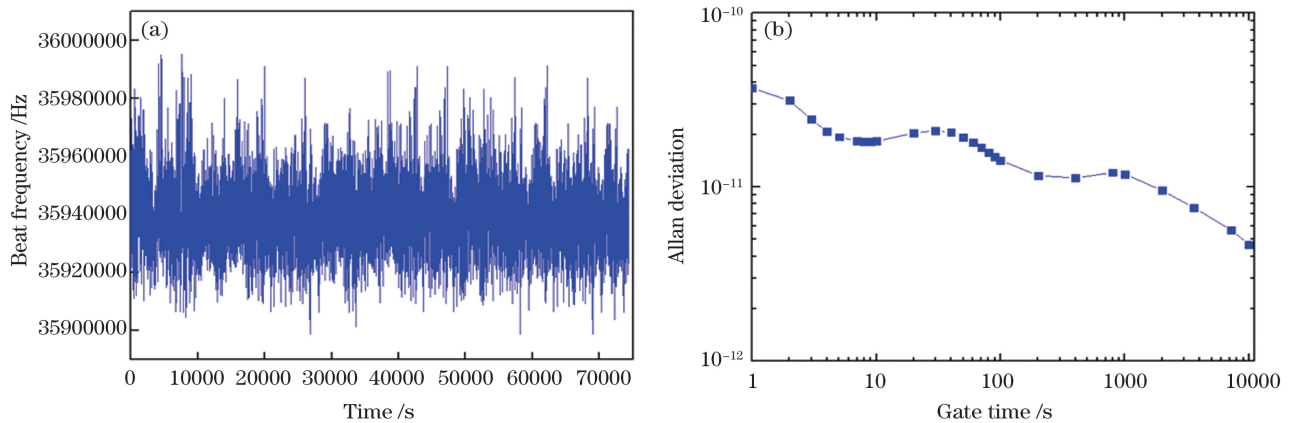


图 7 频率稳定性测试结果。(a)20 h 激光器的频率漂移峰峰值;(b)10000 s 的阿伦方差

Fig. 7 Experimental results of frequency stability. (a) Peak to peak amplitude of frequency fluctuation in 20 h; (b) Allan deviation within 10000 s

5 结 论

理论分析了不同偏振方向的探测光和泵浦光在 $\text{Rb}^{87} \text{D}_2$ 线的超精细谱线 $5^2\text{S}_{1/2} (F_g = 1) \rightarrow 5^2\text{P}_{3/2} (F_e = 0, 1, 2)$ 跃迁上 MTS 误差信号线型不同的原因。研究了铷泡的吸收长度对频率稳定性的影响。采用调制转移光谱稳频技术将激光频率锁定在 $\text{Rb}^{87} \text{D}_2$ 线的超精细谱线 $5^2\text{S}_{1/2} (F_g = 1) \rightarrow 5^2\text{P}_{3/2} (F_e = 0, 1)$ 交叉共振峰上, 20 h 激光器的频率漂移峰峰值为 105 kHz, 积分时间为 1 s 的阿伦方差为 3.7×10^{-11} , 10000 s 的阿伦方差为 4.6×10^{-12} , 满足了冷原子平台对冷却 Rb 原子所需的重泵浦光频率稳定性需求。

参 考 文 献

- [1] Lan X J. Laser technology [M]. Beijing: Science Press, 2000.
蓝信钜. 激光技术[M]. 北京: 科学出版社, 2000.
- [2] Du J, Sun Y G, Chen D J, et al. Research of a compact iodine-stabilized diode laser at 1064 nm [J]. Chinese Journal of Lasers, 2018, 45(7): 0701006.
杜娟, 孙延光, 陈迪俊, 等. 小型化碘稳频 1064 nm 半导体激光器研究 [J]. 中国激光, 2018, 45(7): 0701006.
- [3] Wang J, Chen D J, Wei F, et al. Research on frequency stabilization technology of transfer cavity based on all-fiber ring resonator [J]. Chinese Journal of Lasers, 2020, 47(9): 0906005.
王吉, 陈迪俊, 魏芳, 等. 基于全光纤环形谐振腔的转移腔稳频技术研究 [J]. 中国激光, 2020, 47(9): 0906005.
- [4] Lin B K, Cao S Y, Zhao Y, et al. A compact iodine-stabilized solid-state laser at 532 nm [J]. Chinese Journal of Lasers, 2014, 41(9): 0902002.
林百科, 曹士英, 赵阳, 等. 小型化碘稳频 532 nm 固体激光器 [J]. 中国激光, 2014, 41(9): 0902002.
- [5] Ikegami T, Sudo S, Sakai Y. Frequency stabilization of semiconductor laser diodes [J]. Physical Review A, 1995, 64(1): 289-293.
- [6] Corwin K L, Lu Z T, Hand C F, et al. Frequency-stabilized diode laser with the Zeeman shift in an atomic vapor [J]. Applied Optics, 1998, 37(15): 3295-3298.
- [7] Wieman C, Hänsch T W. Doppler-free laser polarization spectroscopy [J]. Physical Review Letters, 1976, 36(20): 1170-1173.
- [8] Bjorklund G C. Frequency-modulation spectroscopy: a new method for measuring weak absorptions and dispersions [J]. Optics Letters, 1980, 5(1): 15-17.
- [9] Black E D. An introduction to Pound - Drever - Hall laser frequency stabilization [J]. American Journal of Physics, 2001, 69(1): 79-87.
- [10] Preston D W. Doppler-free saturated absorption: laser spectroscopy [J]. American Journal of Physics, 1996, 64(11): 1432-1436.
- [11] Shirley J H. Modulation transfer processes in optical heterodyne saturation spectroscopy [J]. Optics Letters, 1982, 7(11): 537-539.
- [12] Kovachy T, Chiow S W, Kasevich M A. Adiabatic-rapid-passage multiphoton Bragg atom optics [J]. Physical Review A, 2012, 86: 011606.
- [13] Qi X H, Chen W L, Yi L, et al. Ultra-stable rubidium-stabilized external-cavity diode laser based on the modulation transfer spectroscopy technique [J]. Chinese Physics Letters, 2009, 26(4): 044205.
- [14] Han Y S, Wen X, Bai J D, et al. Laser frequency stabilization of 1560 nm laser after frequency doubling to 780 nm with a waveguide: radio-frequency

frequency-modulation spectroscopy versus modulation transfer spectroscopy with Rb atoms[J]. *Acta Optica Sinica*, 2014, 34(5): 0530002.

韩亚帅, 温馨, 白建东, 等. 采用铷原子射频频率调制光谱与调制转移光谱对 1560 nm 激光经波导倍频至 780 nm 进行稳频的比较[J]. *光学学报*, 2014, 34(5): 0530002.

[15] Luan G J, Mao H C, Shi X H. Method for modulating transfer spectrally stabilized laser frequency based on Rb⁸⁷ [J]. *Optics & Optoelectronic*

Technology, 2020, 18(2): 83-86.

栾广建, 毛海岑, 石晓辉. 基于 Rb⁸⁷ 的调制转移光谱稳定激光器频率的方法 [J]. *光学与光电技术*, 2020, 18(2): 83-86.

[16] Noh H R, Park S E, Li L Z, et al. Modulation transfer spectroscopy for ⁸⁷Rb atoms: theory and experiment [J]. *Optics Express*, 2011, 19(23): 23444-23452.

[17] Koester C J, Snitzer E. Amplification in a fiber laser [J]. *Applied Optics*, 1964, 3(10): 1182-1186.

Research on Frequency Stabilization Technology of Modulation Transfer Spectroscopy Based on Rb⁸⁷

Hong Yi^{1,2}, Hou Xia¹, Chen Dijun^{1,3}, Zhou Cuiyun¹, Huang Minjie¹,
Song Tieqiang¹, Wang Guibing¹, Zhao Jian¹, Chen Weibiao¹

¹Spaceborne Laser Engineering Department, Shanghai Institute of Optics and Fine Mechanics,
Chinese Academy of Sciences, Shanghai 201800, China;

²University of Chinese Academy of Sciences, Beijing 100049, China;

³Hangzhou Institute for Advanced Study, University of Chinese Academy of Sciences, Hangzhou, Zhejiang 310024, China

Abstract

Objective Compared with the traditional 780 nm saturated absorption spectroscopy, modulation transfer spectroscopy has higher sensitivity and resolution. It is very suitable for laser frequency stabilization. Nowadays, most of the researchers focus their attention on the hyperfine D₂ line 5²S_{1/2} (F_g = 2) → 5²P_{3/2} (F_e = 3) of Rb⁸⁷ modulation transfer spectrum frequency stabilization technology. However, there are few reports on the hyperfine D₂ line 5²S_{1/2} (F_g = 1) → 5²P_{3/2} (F_e = 0, 1, 2). The main reason is that the saturation absorption peak and error signal amplitude of the latter are much smaller than the former. But the frequency of hyperfine D₂ line 5²S_{1/2} (F_g = 1) → 5²P_{3/2} (F_e = 0, 1) cross resonance peak of Rb⁸⁷, which is suitable for the re-pumping laser needed by cold atomic clock system to cool rubidium atoms, has great research significance. Therefore, it is necessary for us to study it.

Methods By main oscillator power amplifier and efficient frequency doubling of 1560 nm distributed feedback laser with a periodically poled lithium niobate (PPLN) crystal, we have obtained a 780 nm laser about 200 mW. We mix the modulated probe laser with the local signal and get the error signal of modulation transfer spectrum. In order to get better signal-noise ratio (SNR), the signal is amplified and passed by a low-pass-filter. We also change the modulation frequency and modulation depth of electro-optic modulator (EOM) to increase the amplitude of the error signal. The laser frequency is locked to the D₂ hyperfine transition 5²S_{1/2} (F_g = 1) → 5²P_{3/2} (F_e = 0, 1) of Rb⁸⁷ via proportional-integral-derivative (PID) controller and we get a 20 h laser frequency stability data finally. We change the polarization of probe laser and pump laser by adjusting the optical structure, so as to study the influence of different polarization states on the error signal of modulation transfer spectrum. By changing the absorption length of rubidium cell (25 mm and 50 mm), we study its effect on laser frequency stability.

Results and Discussions We find that the error signal on the hyperfine D₂ line 5²S_{1/2} (F_g = 1) → 5²P_{3/2} (F_e = 0, 1, 2) of Rb⁸⁷ can be influenced by different polarization of probe laser and pump laser. Only when the probe laser and pump laser are linearly polarized in the same direction can there be a clear and large single error signal on the D₂ hyperfine transition 5²S_{1/2} (F_g = 1) → 5²P_{3/2} (F_e = 0, 1) of Rb⁸⁷ (Fig. 3). There will be no locking error on this transition compared with probe laser and pump laser are perpendicular polarized or circular polarization. We finally lock the laser frequency on this transition for 20 h and measure laser frequency is 384234489.5 MHz (the theoretical calculation is 384234490.2 MHz, with a difference of 0.7 MHz). The peak to peak amplitude of frequency

fluctuation is 105 kHz in 20 h. The Allan deviation of the frequency stability is 3.7×10^{-11} when the integration time is 1 s and 4.6×10^{-12} when the integration time is 10000 s (Fig. 7). The influence of rubidium cell absorption length on frequency stability is studied. We find the amplitude of error signal in 50 mm is higher than that in 25 mm (Fig. 5). The 1 h frequency fluctuation of rubidium cell in 50 mm is 80 kHz, which is less than that in 25 mm (152 kHz). The 1 s frequency stability of rubidium cell in 50 mm is 3.7×10^{-11} , which is also less than that in 25 mm (5.4×10^{-11}), but 1000 s frequency stability about the same (Fig. 6). The results show that increasing the absorption length of a single rubidium cell will produce a higher SNR, which will be beneficial to the short-term laser frequency stability. However, its effect on the long-term laser frequency stability is not significant. Perhaps the long-term laser frequency stability depends on other factors, such as the temperature control of rubidium cell and EOM.

Conclusions The reason for the difference of modulation transfer spectroscopy (MTS) error signal, which is caused by probe laser and pump laser in different polarization directions, on the hyperfine D_2 line $5^2S_{1/2}(F_g = 1) \rightarrow 5^2P_{3/2}(F_e = 0, 1, 2)$ of Rb^{87} is analyzed theoretically. The influence of the absorption length of rubidium cell on the frequency stability is studied. The laser frequency is locked on the D_2 hyperfine transition $5^2S_{1/2}(F_g = 1) \rightarrow 5^2P_{3/2}(F_e = 0, 1)$ of Rb^{87} via modulation transfer spectroscopy. The results show that the peak to peak frequency fluctuation is 105 kHz in 20 h. The Allan deviation of the frequency stability is 3.7×10^{-11} when the integration time is 1 s and 4.6×10^{-12} when the integration time is 10000 s, which meets the requirement of cold atom platform for cooling atoms.

Key words laser optics; laser frequency stabilization; modulation transfer spectroscopy; feedback laser; polarization; ultra-cold atoms

OCIS codes 140.3425; 140.3515